Wind-Wave Nonlinearity Observed at the Sea Floor. Part II: Wavenumbers and Third-Order Statistics

T. H. C. HERBERS AND R. T. GUZA

Center for Coastal Studies, Scripps Institution of Oceanography, La Jolla, California

(Manuscript received 6 May 1991, in final form 12 August 1991)

ABSTRACT

This is Part 2 of a study of nonlinear effects on natural wind-generated surface gravity waves in 13-m depth, 30 km offshore of Virginia. At the sea floor in this depth, free surface gravity waves are only weakly attenuated at sea and swell frequencies (0.05–0.30 Hz) but are very strongly attenuated at frequencies higher than about 0.35 Hz. Hence, above 0.35 Hz, relatively long wavelength forced waves, excited by nonlinear interactions between directionally opposing free wind waves, are exposed at the sea floor. An array of pressure transducers at middepth was used to estimate the frequency–directional spectrum of (free) primary sea and swell waves, and the associated (forced) secondary pressure fluctuations were measured with an array on the sea floor. In Part 1, it was shown that forced-wave energy levels at the sea floor increase sharply in response to directionally opposing wind waves, in agreement with weakly nonlinear theory. In Part 2, wavelengths, propagation directions, and non-Gaussian phase coupling between free and forced waves are examined on three occasions with relatively high forced-wave energy levels.

A root-mean-square wavenumber magnitude and a vector-averaged mean wave propagation direction (both functions of frequency) can be expressed accurately in terms of the pressure array cross-spectra. The wavenumber estimates at the sea floor show the theoretically expected sharp transition between a 0.05–0.30 Hz frequency range dominated by free sea and swell waves and a 0.35–0.60 Hz range dominated by forced waves with wavelengths that are long relative to free waves of the same frequency. In the "free-wave frequency range," wavenumber estimates are usually well within 10% of the linear dispersion relation and wave direction estimates are in excellent agreement with the directional spectra extracted from the middepth array. In the "forced-wave frequency range," wavenumber and direction estimates agree with nonlinear theory predictions, confirming that the observed forced waves have the sum vector wavenumber of the interacting directionally opposing wind waves.

Phase coupling between free and forced waves is examined through third-order statistics of the sea floor pressure data. Consistent with theory, the normalized bispectrum has small imaginary parts scattered approximately randomly about zero and relatively large negative real parts at frequencies that correspond to directionally opposing seas and swell. Estimates of the bispectrum integrated for constant sum frequency confirm that nearly all the energy at double sea frequencies is nonlinearly coupled to directionally opposing wind waves. In qualitative agreement with nonlinear theory predictions, bispectral levels are sometimes significantly reduced by directional spreading of the interacting free waves.

1. Observations of secondary waves on the sea floor

Theories for weakly nonlinear wind-generated surface gravity waves, based on a perturbation expansion for small wave steepness, show that the lowest order nonlinear (triad) interactions do not support resonances (e.g., Phillips 1960; Hasselmann 1962; and others). Two primary (free) wave components with vector wavenumbers $\mathbf{k}_1$ and $\mathbf{k}_2$ and frequencies f_1 and f_2, obeying the dispersion relation

$$f = \frac{1}{2\pi}\,[gk\,\tanh(kh)]^{1/2}, \qquad (1)$$

with k the wavenumber magnitude ($\mathbf{k} = [k\cos\theta, k\sin\theta]$), θ the wave propagation direction, g the acceleration of gravity, and h the water depth, excite secondary (forced) wave components with the sum and difference wavenumber and frequency ($\mathbf{k}_1 \pm \mathbf{k}_2, f_1 \pm f_2$; for $f_1 \geq f_2$) not obeying the dispersion relation. Resonances first occur in quartet interactions between three primary wave components and a tertiary wave component, causing weak nonlinear energy transfers of crucial importance to the evolution of wind wave spectra (e.g., Hasselmann et al. 1973).

The present work concerns high-frequency secondary waves excited by sum interactions of two primary wave components. Secondary waves have little dynamical significance but dominate the local nonlinearity of surface gravity waves. Depending on the wavenumbers $\mathbf{k}_1$ and $\mathbf{k}_2$ of the interacting primary wave pair, a forced secondary wave can have a wavelength very different from free waves of the same frequency, as has been observed at double wind wave frequencies

Corresponding author address: Dr. Thomas H. C. Herbers, Scripps Institution of Oceanography, Center for Coastal Studies, A-009, La Jolla, CA 92093-0209.

in laboratory experiments (e.g., Mitsuyasu et al. 1979; Donelan et al. 1985). It is well known that secondary wave components are important to wind wave statistics (e.g., Longuet-Higgins 1963). Free primary wave components, generated at different times and locations by unrelated wind forces on the sea surface, can be assumed to be statistically independent. Thus, according to the central limit theorem, wind wave statistics are approximately Gaussian, in agreement with many observations (e.g., Kinsman 1965). Nonlinear triad interactions cause nonzero third-order statistics, owing to a consistent relationship between the amplitudes and phases of a secondary wave component and the corresponding pair of primary wave components. This coupling of free and forced waves typically results in a visually appealing skewed sea surface profile with peaky crests and flat troughs and complicates the interpretation of remote sensing data. The deviations from the dispersion relation and non-Gaussian statistics associated with the secondary wave field can cause errors in the analysis of wind wave data, often based on linear wave theory.

Near the sea surface, forced-wave energy is often at least an order of magnitude smaller than free-wave energy (e.g., Komen 1980; Donelan et al. 1985; Laing 1986). However, surface gravity waves are very strongly attenuated at depths exceeding their wavelength. Thus, free sea and swell waves are confined, depending on their frequency, to roughly the upper 5–500 m of the ocean. On the other hand, forced secondary waves at sum frequencies can have very long wavelengths if generated in triad interactions with two primary waves of nearly equal frequency traveling in opposing directions ($\mathbf{k}_1 \approx -\mathbf{k}_2$; Miche 1944). These virtually unattenuated long-wavelength forced waves theoretically dominate the high-frequency wave pressure field at great depths and are believed to be a principal generation mechanism for sea floor microseisms (e.g., Longuet-Higgins 1950; Hasselmann 1963; Webb and Cox 1986; Cox and Jacobs 1989; Goodman et al. 1989).

This is Part 2 of a field study [Part 1, Herbers and Guza (1991), is hereafter referred to as HG1] of high-frequency secondary waves using observations collected as part of the SAXON (SAR and X-band Ocean Nonlinearities) Experiment. Two arrays of pressure transducers were deployed in 13-m depth at the Chesapeake Light Tower, located in the Atlantic Ocean about 30 km offshore of the mouth to Chesapeake Bay. A 20 m $\times$ 20 m aperture array was mounted on the tower structure at middepth to provide estimates of the free-wave frequency–directional spectrum. These estimates are used together with weakly nonlinear theory to predict the secondary pressure field at the sea floor. The forced-wave predictions are compared to observations made with a smaller (12 m $\times$ 12 m aperture) array, buried a few centimeters in the sand and displaced 24 m east of the Chesapeake Light Tower. The details of the experiment are described in HG1. The water depth at this site has the advantage that the vertical decay of free waves at typical wind wave frequencies (0.2–0.3 Hz) is weak, while free waves at double wind wave frequencies are very strongly attenuated at the sea floor. At 0.2 Hz free-wave energy at middepth is reduced by 0.14 relative to the surface, compared to a 2×10^{-7} reduction at 0.4 Hz at the sea floor. The water column filters out the high-frequency part of the free-wave spectrum and longer-wavelength forced secondary waves are theoretically expected to dominate the sea floor pressure field at double wind-wave frequencies (0.4–0.6 Hz). Pressure data was collected nearly continuously from 17 September through 14 October 1988, with a sample frequency of 2 Hz. The present study is focused on data acquired between 9 and 13 October. In this 85-h period, forced-wave energy levels fluctuated by as much as two orders of magnitude on time scales of only a few hours (HG1).

The observed variability of forced-wave energy is related to changes in directional properties of free wind waves. Although forced waves generated by sum interactions of nearly colinear free waves ($\theta_1 \approx \theta_2$) in 13-m depth have wavelengths long relative to free waves of the same frequency, these forced waves are still not long compared to the water depth ($|\mathbf{k}_1 + \mathbf{k}_2|\, h \gg 1$) and therefore are strongly attenuated at the sea floor. Hence, forced-wave energy levels at the sea floor are theoretically expected to be relatively weak in unidirectional seas and to increase dramatically when directionally opposing seas ($|\mathbf{k}_1 + \mathbf{k}_2|\, h \leqslant \mathrm{O}(1)$) are present. Figures 1, 2, and 3 (reproduced from HG1) show estimates of the bottom-pressure frequency spectrum $E_b(f)$, and the surface elevation frequency–directional spectrum of (free) sea and swell waves $E_{s,\mathrm{free}}(f, \theta)$, obtained from 2-hour records collected on 11, 12, and 13 October, respectively, when high-frequency forced-wave energy levels were at a maximum. On 12 October, directionally opposing seas of slightly different frequency (approximately 0.2 Hz and 0.25 Hz, Fig. 2b), generated by a sudden veering of the local wind direction from south to north (HG1), excite a pronounced forced-wave peak in $E_b(f)$ at the sum frequency (0.45 Hz, Fig. 2a). On the other hand, the 0.5-Hz and 0.4-Hz forced-wave peaks observed on 11 October (Fig. 1a) and 13 October (Fig. 3a), respectively, are not associated with a veering in local winds, but result from interactions between locally generated wind waves and nonlocally generated high-frequency seas (radiating from the mouth of Chesapeake Bay located to the northwest) traveling in a different direction (Figs. 1b and 3b, respectively). Energy levels of high-frequency forced waves were dramatically lower during periods of more unidirectional waves (HG1). Predictions of the high-frequency secondary wave spectrum based on weakly nonlinear theory (Hasselmann 1962) and the $E_{s,\mathrm{free}}(f, \theta)$ estimates are consistent with the observed large [O (10^2)] fluctuations in forced-wave energy (HG1). Discrepancies be-

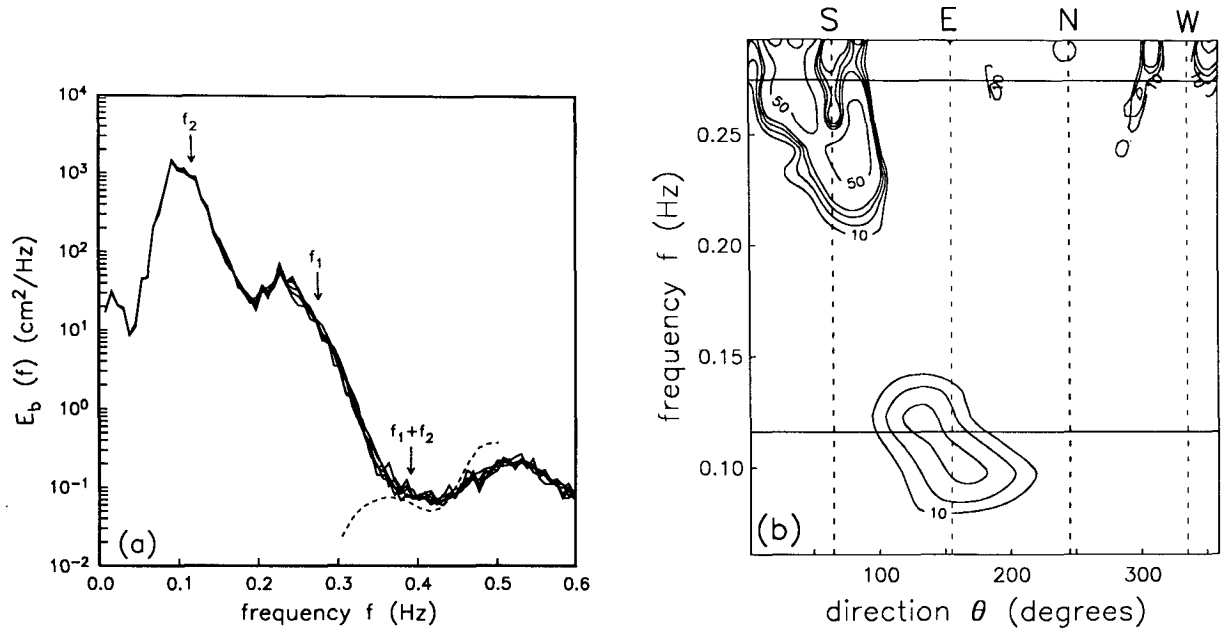

FIG. 1. Forced-wave energy and free-wave directions on 11 October 1988 (HG1). (a) Observed sea floor pressure frequency spectra $E_b(f)$ of all instruments (solid curves) and a theoretical prediction of the forced secondary wave spectrum (dashed). (b) An estimate of the surface elevation frequency–directional spectrum of free primary waves $E_{s,\text{free}}(f, \theta)$. Contour levels are 10, 15, 20, 25, 50, 75, 100, 150, 200, and 250 cm²/Hz°. The wave propagation direction θ is defined in Fig. 4. The arrows in (a) and solid lines in (b) indicate the frequencies corresponding to the peak of the observed (normalized) bispectrum $b(f_1, f_2)$.

tween the predicted and observed forced-wave energy levels at the sea floor (Figs. 1a, 2a, and 3a) may result from the very limited directional resolution of the middepth array.

In the present paper, wavenumbers of free and forced waves and non-Gaussian statistics observed at the sea floor are compared to predictions based on weakly nonlinear theory (Hasselmann 1962) and the middepth

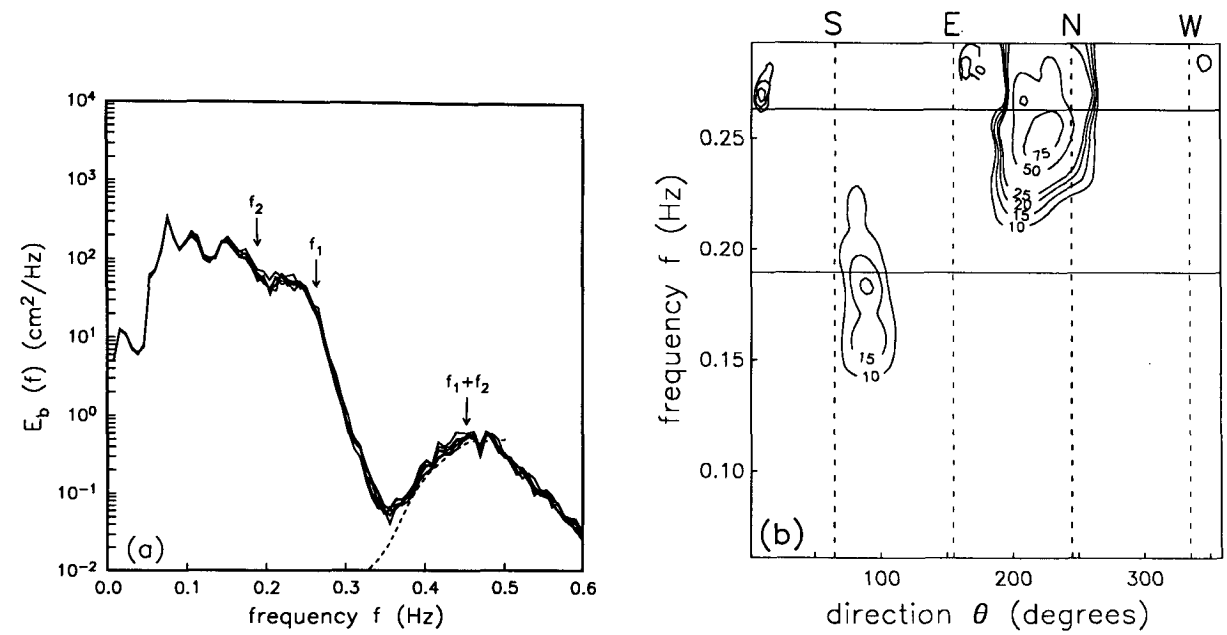

FIG. 2. As in Fig. 1 but on 12 October 1988.

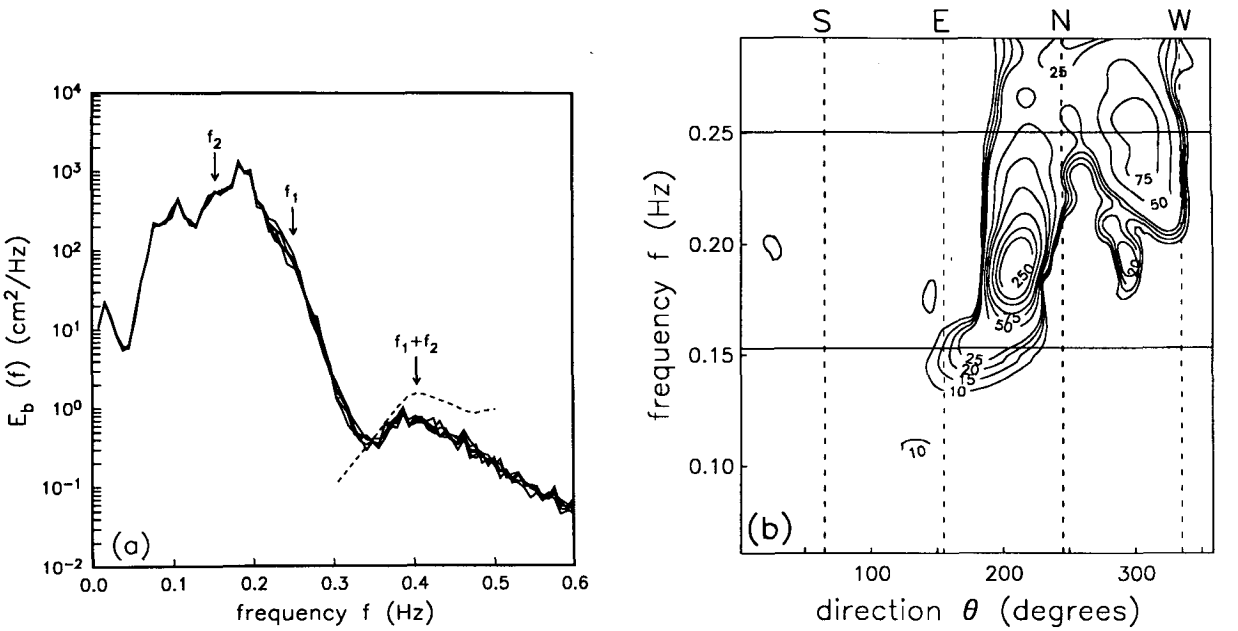

FIG. 3. As in Fig. 1 but on 13 October 1988.

$E_{s,\text{free}}(f, \theta)$ estimates. Estimates of an average wavenumber magnitude and propagation direction (both functions of frequency) are compared to nonlinear theory predictions in section 2. Non-Gaussian statistics associated with phase-coupling between free and forced waves are discussed in section 3 and examined in the sea floor pressure observations through estimates and nonlinear theory predictions of the bispectrum in section 4. The results are summarized in section 5.

2. Average wavenumbers and propagation directions

The interpretation of multicomponent measurements of surface gravity waves in the ocean is often based on the assumption that forced-wave contributions are negligible and wave statistics can be fully described by a surface elevation frequency–directional spectrum $E_{s,\text{free}}(f, \theta)$ of free-wave components obeying the linear dispersion relation between wavenumber magnitude k and frequency f [Eq. (1)]. From a limited number of instruments, relatively precise estimates of $E_{s,\text{free}}(f, \theta)$ can be extracted with a variety of methods. The inverse technique used in the present study minimizes a roughness norm of the directional spreading function subject to the constraints that the estimate is nonnegative and fits the array cross-spectra within a chosen (75%) statistical confidence level (Herbers and Guza 1990). Estimates of $E_{s,\text{free}}(f, \theta)$ (Figs. 1b, 2b, and 3b) were obtained from the middepth pressure array data with this technique in the (sea and swell) frequency range 0.05–0.30 Hz (HG1). Although consistent with the data, these directional spectra estimates possibly have large errors due to the limited resolving power of the (20 m × 20 m aperture) array and only qualitatively describe the directional properties of free waves (HG1). Another potential source of errors in $E_{s,\text{free}}(f, \theta)$ estimates are forced-wave contributions to the array cross-spectra that do not obey the dispersion relation [Eq. (1)]. An assumption of free-wave dominance is theoretically justified near the spectral peak frequency where forced-wave contributions are relatively weak. However, because free waves at double sea frequencies are very strongly attenuated at the sea floor, the observed bottom-pressure oscillations in the frequency range of about 0.35–0.60 Hz (Figs. 1a, 2a, and 3a) must have wavelengths radically different from the linear dispersion relation (HG1). To verify the assumed free-wave dominance at sea and swell frequencies, and to compare the observed wavelengths and directions of higher-frequency forced waves to theoretical predictions, array analysis is needed that relaxes the assumption of a dispersion relation between k and f.

Wavelengths and propagation directions of free- and forced-wave components can in principle be examined at the sea floor through the bottom-pressure (vector) wavenumber–frequency spectrum $E_b(f, k, \theta)$ (used below in polar form), but meaningful estimates of $E_b(f, k, \theta)$ require a much more extensive array than the six-element pressure sensor array deployed on the sea floor at the Chesapeake Light Tower (Fig. 4). However, owing to its compact geometry, accurate estimates of a root-mean-square wavenumber magnitude k_{rms},

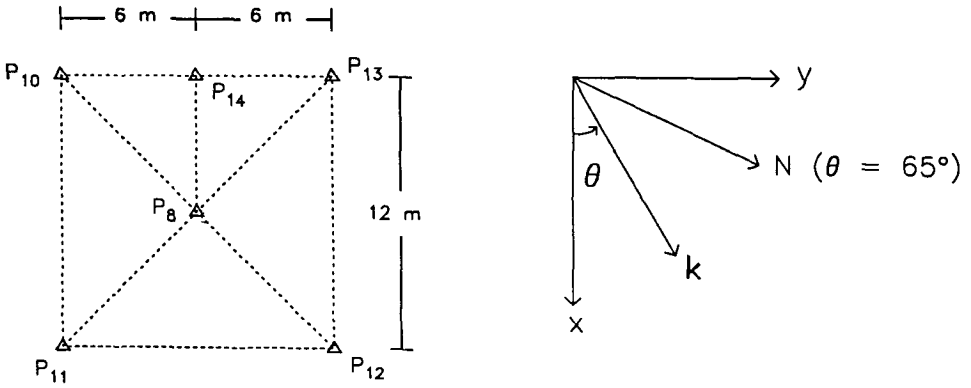

FIG. 4. Geometry of the bottom-pressure sensor array and analysis coordinate frame.

$$k_{\mathrm{rms}}(f) \equiv \left[\frac{\int_0^{\infty} dk \int_0^{2\pi} kd\theta k^2 E_b(f, k, \theta)}{\int_0^{\infty} dk \int_0^{2\pi} kd\theta E_b(f, k, \theta)} \right]^{1/2} \quad (2)$$

and a vector-averaged mean wave direction θ_{mean},

$$\tan[\theta_{\mathrm{mean}}(f)] \equiv \frac{\int_0^{\infty} dk \int_0^{2\pi} kd\theta k \sin(\theta) E_b(f, k, \theta)}{\int_0^{\infty} dk \int_0^{2\pi} kd\theta k \cos(\theta) E_b(f, k, \theta)} \quad (3)$$

(both funtions of frequency) can be extracted from the array cross-spectra. The estimation technique is based on an expansion for small sensor separations relative to the wavelength, analogous to Herbers and Guza (1989). The accuracy of the k_{rms} and θ_{mean} estimates presented below is somewhat limited because the six-element bottom array simply does not have optimal lags for the shortest and longest wavelengths expected at the sea floor. Nonetheless, errors in k_{rms} and θ_{mean} estimates are expected to be small enough for qualitative comparisons to weakly nonlinear theory. The details of the estimators and a discussion of their accuracy is given in appendix A.

Estimates of $k_{\mathrm{rms}}(f)$ and $\theta_{\mathrm{mean}}(f)$ [appendix A, Eq. (A5)], extracted from 136.5-minute-long bottom-pressure records (the cross-spectra have approximately 200 degrees of freedom) collected on 11, 12, and 13 October 1988 (when forced-wave energy levels were relatively high; Figs. 1, 2, and 3), are shown in Figs. 5, 6, and 7. The observed wavenumbers agree well with the theoretical dispersion relation for free surface gravity waves [Eq. (1)] at sea and swell frequencies (0.05–0.30 Hz; Figs. 5a, 6a, and 7a), with (normalized) deviations from the linear wavenumber generally within 10% (Fig. 8). In all three cases the $k_{\mathrm{rms}}(f)$ estimates are within a few percent of the dispersion relation in the range 0.08–0.14 Hz. At lower frequencies (0.05–0.08 Hz) the discrepancies are slightly larger (5%–10%), possibly because the estimates are more sensitive to measurement errors for relatively long wavelength swell. The deviations of $k_{\mathrm{rms}}(f)$ estimates from the linear wavenumber are also slightly larger at sea frequencies, from about 5% in the range 0.14–0.25 Hz to 10% for $f = 0.3$ Hz. Simulations suggest that the observed slight divergence from the dispersion relation in the frequency range 0.25–0.30 Hz, although qualitatively consistent with a small contribution of (long-wavelength) forced secondary waves, may be caused by the bias expected for (short-wavelength) free high-frequency seas (appendix A). Overall, in the range 0.05–0.30 Hz, the observed small deviations from linear dispersion are well within the expected accuracy of the estimates and confirm that this frequency range is indeed dominated by free primary waves, as was assumed in the estimation of $E_{s,\mathrm{free}}(f, \theta)$ (HG1).

As a consistency check on the accuracy of the data and the analysis technique, $\theta_{\mathrm{mean}}(f)$ was also independently estimated from the middepth array, in the "free-wave frequency range" 0.05–0.30 Hz (assuming linear dispersion), through integration of the $E_{s,\mathrm{free}}(f, \theta)$ estimates (Figs. 1b, 2b, and 3b)

$$\tan[\theta_{\mathrm{mean,free}}(f)] = \frac{\int_0^{2\pi} d\theta \sin(\theta) E_{b,\mathrm{free}}(f, \theta)}{\int_0^{2\pi} d\theta \cos(\theta) E_{b,\mathrm{free}}(f, \theta)} \quad (4)$$

with $E_{b,\mathrm{free}}(f, \theta)$ ($= [\cosh(kh)]^{-2} E_{s,\mathrm{free}}(f, \theta)$) the bottom-pressure frequency–directional spectrum of free waves. In all three cases (Figs. 5b, 6b, and 7b) the independent (i.e., different arrays and analysis methodologies) θ_{mean} estimates are in excellent agreement, suggesting that the effects of measurement inaccuracies (e.g., finite array size bias, instrument noise, and sensor positioning errors) on k_{rms} and θ_{mean} estimates are small.

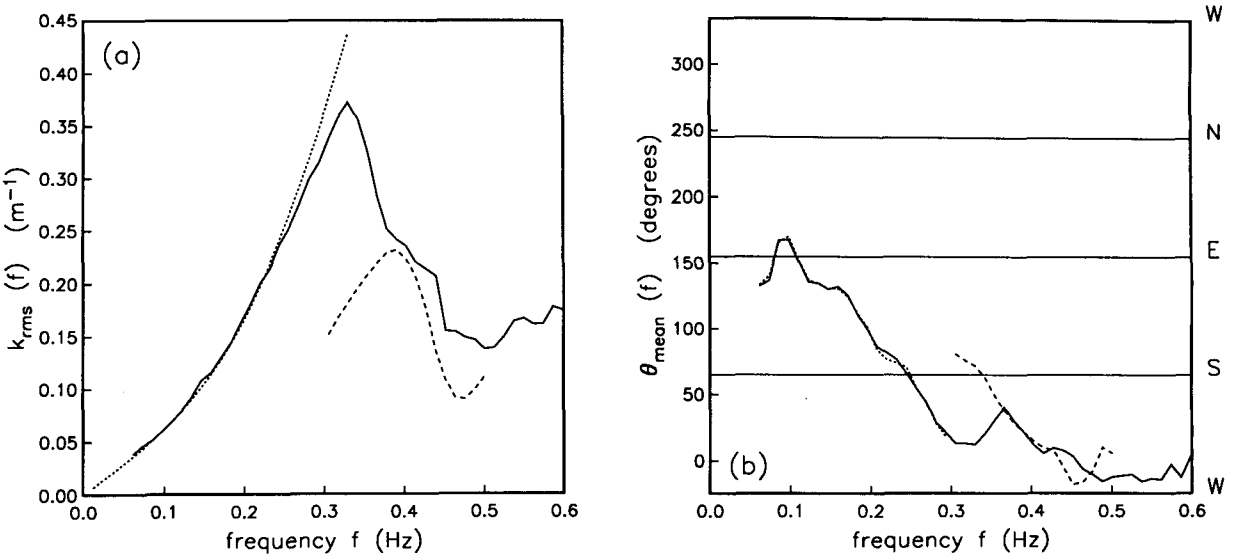

FIG. 5. Root-mean-square wavenumber magnitude and mean wave propagation direction of sea floor pressure, as a function of frequency, on 11 October 1988. (a) The solid curve is an estimate of $k_{rms}(f)$ based on the bottom array observations [appendix A, Eq. (A5a)], the dotted curve is the surface gravity wave dispersion relation [Eq. (1)], and the dashed curve is a nonlinear theory prediction of $k_{rms,\,forced}(f)$ [Eq. (5a)]. (b) The solid curve is an estimate of $\theta_{mean}(f)$ based on the bottom array observations [appendix A, Eq. (A5b)], the dotted curve is an estimate of $\theta_{mean,\,free}(f)$ obtained by integrating $E_{s,\,free}(f, \theta)$ [Eq. (4), based on middepth measurements], and the dashed curve is a theoretical prediction of $\theta_{mean,\,forced}(f)$ [Eq. (5b)].

At frequencies above 0.3 Hz (where free waves are strongly attenuated at the sea floor), the estimated values of $k_{rms}(f)$ drop very sharply and are minimum at approximately the forced-wave peak frequency (compare Figs. 5a, 6a, and 7a with Figs. 1a, 2a, and 3a). Between 0.30 and 0.35 Hz the surface-to-bottom attenuation of the free-wave spectrum changes from 3×10^{-4} to 10^{-5}, causing a sharp transition in k_{rms} estimates between free-wave dominance for $f < 0.30$ Hz and forced-wave dominance for $f > 0.35$ Hz on all three days. According to the nonlinear interaction rule for wave triads, forced secondary wave components

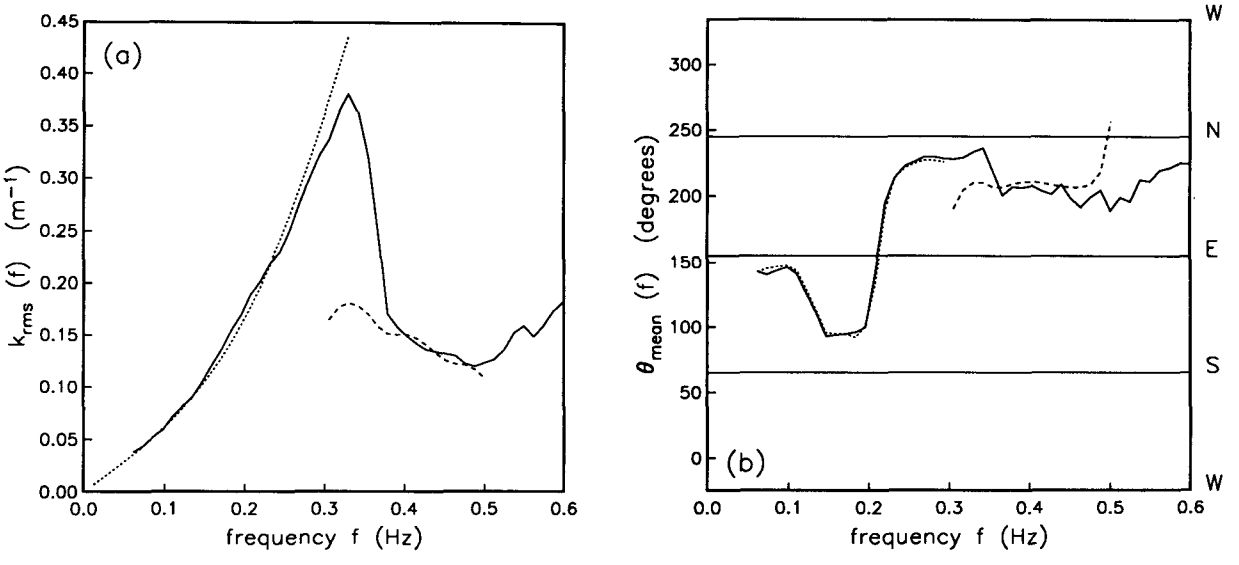

FIG. 6. As in Fig. 5 but on 12 October 1988.

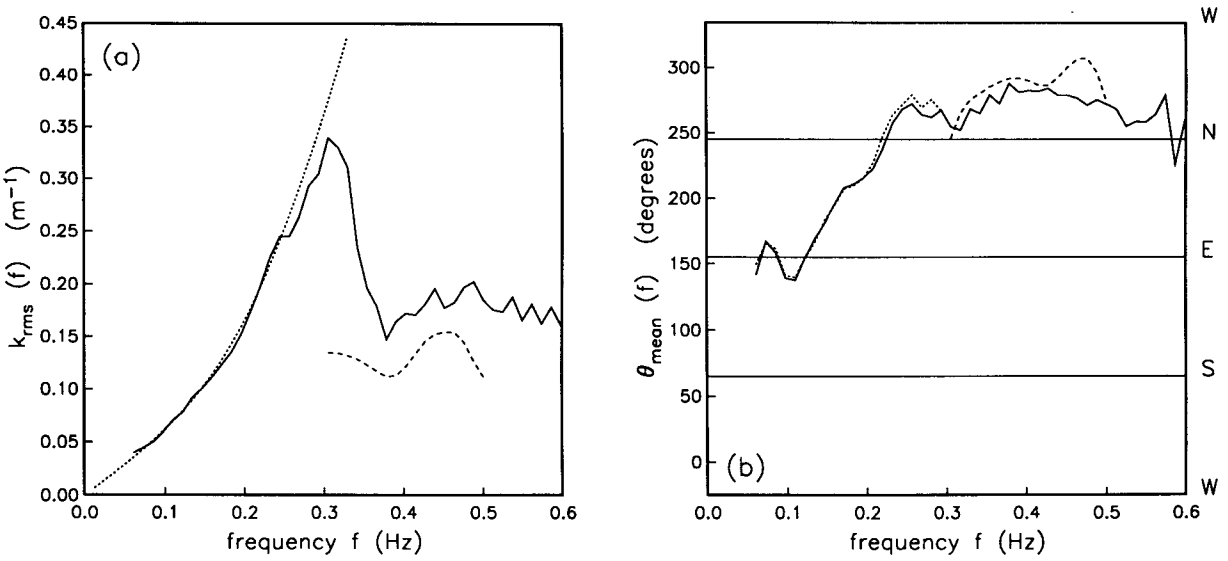

FIG. 7. As in Fig. 5 but on 13 October 1988.

have the sum frequency and vector wavenumber of the corresponding pair of free primary waves. Hence, free waves with about the same frequency traveling in nearly opposing directions excite relatively long wavelength (i.e., weakly attenuated) high-frequency forced waves, traveling in a predictable direction. The observed forced wavenumber magnitudes are indeed generally smaller than or comparable to the linear wavenumber magnitudes of the dominant (0.15–0.30 Hz) free wind waves (Figs. 5a, 6a, and 7a). Estimates of $\theta_{mean}(f)$ (Figs. 5b, 6b, and 7b) show large variations in mean forced-wave propagation directions between 11 and 13 October, in response to changes in $E_{s,free}(f, \theta)$ (compare Figs. 1b, 2b, and 3b). On 11 October (Fig. 5b) θ_{mean} ranges from southwest for 0.35-Hz forced waves, excited by interactions between seas from the southwest and swell from the east, to west for 0.5-Hz forced waves, generated in interactions between seas arriving from the south and northwest (Fig. 1b). On 12 October (Fig. 6b) forced waves arrive from the northeast, consistent with the sum vector wavenumber of nearly directionally opposing seas (generated after a sudden shift in wind direction, HG1) arriving from the north and southeast (Fig. 2b). On 13 October (Fig. 7b) the dominant forced-wave propagation direction is northwest, as expected for interactions between local seas from the northeast and nonlocal seas from the west (radiating from Chesapeake Bay, Fig. 3b).

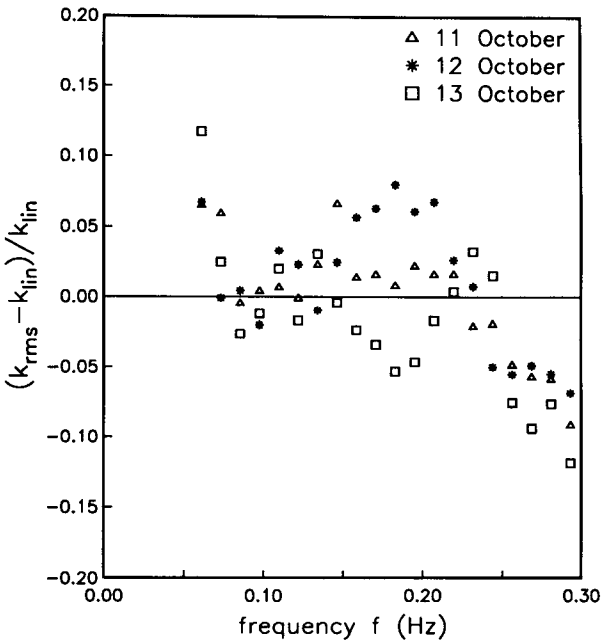

FIG. 8. Normalized deviations of wavenumber estimates from linear dispersion $(k_{rms} - k_{lin})/k_{lin}$, with k_{rms} the estimate based on Eq. (A5a) (appendix A) and k_{lin} the linear wavenumber given by Eq. (1), as a function of frequency in the sea and swell range 0.05–0.30 Hz, on all three days.

The free-wave frequency–directional spectrum estimates (Figs. 1b, 2b, and 3b) can be used, together with the general theory for weakly nonlinear surface gravity waves (Hasselmann 1962; Hasselmann et al. 1963), to predict the wavenumbers and propagation directions of forced sea-floor pressure fluctuations. At high frequencies, dominated by forced secondary waves, $k_{rms}(f)$ [Eq. (2)] and $\theta_{mean}(f)$ [Eq. (3)] are approximately given by (appendix B)

$$k_{\text{rms, forced}}(f) \approx \left[\frac{\int_0^f df' \int_0^{2\pi} d\theta_1 \int_0^{2\pi} d\theta_2 [k_{f'}^2 + k_{f-f'}^2 + 2k_{f'}k_{f-f'}\cos(\Delta\theta)] \times D^2(f', f-f', \Delta\theta) E_{b,\text{free}}(f', \theta_1) E_{b,\text{free}}(f-f', \theta_2)}{\int_0^f df' \int_0^{2\pi} d\theta_1 \int_0^{2\pi} d\theta_2 D^2(f', f-f', \Delta\theta) E_{b,\text{free}}(f', \theta_1) E_{b,\text{free}}(f-f', \theta_2)} \right]^{1/2} \quad (5a)$$

$$\tan[\theta_{\text{mean, forced}}(f)] \approx \frac{\int_0^f df' \int_0^{2\pi} d\theta_1 \int_0^{2\pi} d\theta_2 [k_{f'}\sin(\theta_1) + k_{f-f'}\sin(\theta_2)] \times D^2(f', f-f', \Delta\theta) E_{b,\text{free}}(f', \theta_1) E_{b,\text{free}}(f-f', \theta_2)}{\int_0^f df' \int_0^{2\pi} d\theta_1 \int_0^{2\pi} d\theta_2 [k_{f'}\cos(\theta_1) + k_{f-f'}\cos(\theta_2)] \times D^2(f', f-f', \Delta\theta) E_{b,\text{free}}(f', \theta_1) E_{b,\text{free}}(f-f', \theta_2)} \quad (5b)$$

where D is the nonlinear interaction coefficient [appendix B, Eq. (B3)], k_f denotes the linear wavenumber at frequency f [Eq. (1)], $\Delta\theta = |\theta_1 - \theta_2|$ is the difference in propagation direction of the interacting free waves, and $E_{b,\text{free}}(f, \theta)$ is set equal to zero for $f < 0.05$ Hz and $f > 0.30$ Hz.

Theoretical predictions of $k_{\text{rms, forced}}(f)$ and $\theta_{\text{mean, forced}}(f)$ in the frequency range 0.3–0.5 Hz, based on Eq. (5) and the $E_{b,\text{free}}(f, \theta)$ estimates, are included in Figs. 5, 6, and 7. In all three cases the estimated and predicted wavenumbers and directions agree well at frequencies above about 0.35 Hz, where free-wave contributions to the sea floor pressure field are expected to be negligibly small. The agreement of $k_{\text{rms}}(f)$ estimates with theory is best on 12 October (Fig. 6a), when observed and predicted forced-wave energy levels also show good agreement (Fig. 2a). On 11 and 13 October (with larger discrepancies between observed and predicted forced-wave energy levels; compare Figs. 1a and 3a with Fig. 2a), the predictions of $k_{\text{rms, forced}}(f)$ are about 10%–30% lower than the estimates (Figs. 5a and 7a), possibly due to errors in the $E_{b,\text{free}}(f, \theta)$ estimates associated with the small array aperture (HG1). On all three days, the predicted and observed $\theta_{\text{mean, forced}}(f)$ generally agree to within 15° (Figs. 5b, 6b, and 7b).

In summary, $k_{\text{rms}}(f)$ and $\theta_{\text{mean}}(f)$ estimates confirm that sea and swell are free waves obeying the linear dispersion relation [Eq. (1)] and show that the associated sum frequency forced waves have wavelengths and propagation directions consistent with the nonlinear interaction rule for wave triads. Since estimates of k_{rms} and θ_{mean} are expected to be very sensitive to small measurement errors for $kL \ll 1$ (appendix A), frequencies less than 0.05 Hz are not considered in this study. At frequencies below 0.05 Hz the pressure spectra may contain both locally forced secondary waves excited by difference interactions between seas and swell (e.g., Longuet-Higgins and Stewart 1962) and free (leaky or trapped) waves generated at the shoreline (e.g., Munk et al. 1964). Average wavenumber estimates may be useful to distinguish between these two different sources of low-frequency wave energy and, for example, explain the origin of the 0.01–0.02-Hz peak observed in all three bottom-pressure frequency spectra shown in Figs. 1a, 2a, and 3a. Unfortunately, the aperture of the bottom array is very small compared to the wavelengths expected at these low frequencies ($kL = 0.03$–0.07 for 0.01–0.02-Hz free waves), so that wavenumber estimates may have large errors. Work is in progress to obtain estimates of k_{rms} and θ_{mean} and other bulk parameters from array data collected recently in 13-m depth, offshore of North Carolina. The estimates from this much more extensive (24 elements) and larger-aperture (250 m × 250 m) array are expected to be very accurate for a wide range of wavelengths [O(10 m–1 km)], spanning free sea and swell (0.05–0.35 Hz) and the corresponding (0.01–0.70 Hz) forced secondary waves excited by both sum and difference interactions, as well as nonlocally generated free low-frequency (0.01–0.05 Hz) gravity waves. In addition, the recently collected dataset will be used to obtain estimates of $E_b(f, k, \theta)$ that are expected to be accurate enough to resolve the gross structure of the forced secondary wavenumber spectrum at double sea frequencies.

3. Third-order statistics of sea floor pressure

Natural wind-generated surface gravity waves have approximately Gaussian statistics owing to the statistical independence of primary (free) wave components generated by independent wind forces on the sea surface (e.g., Kinsman 1965). A Gaussian primary wave field implies that the third-order correlation function $R_b(\tau_1, \tau_2)$ of sea floor pressure $p(t)$

$$R_b(\tau_1, \tau_2) \equiv \mathrm{E}\{p(t)p(t+\tau_1)p(t+\tau_2)\} \quad (6)$$

vanishes in the linear approximation. However, forced

secondary wave components, predicted by weakly nonlinear theory [appendix B, Eq. (B2); Hasselmann 1962], introduce non-Gaussian statistics. The amplitudes and phases of a forced-wave component and the two corresponding free-wave components are not statistically independent but are coupled through the interaction coefficient D [appendix B, Eq. (B3)]. Therefore, $R_b(\tau_1, \tau_2)$ generally does not vanish if weak nonlinearity is included. Third-order statistics are of particular interest to the present study because coupled wave triads consisting of one secondary and two primary components contribute the leading order terms in a perturbation expansion of R_b for small wave steepness (Hasselmann et al. 1963):

$$R_b(\tau_1, \tau_2) \approx \mathrm{E}\{p^{(1)}(t)p^{(1)}(t+\tau_1)p^{(2)}(t+\tau_2) + p^{(1)}(t)p^{(2)}(t+\tau_1)p^{(1)}(t+\tau_2) + p^{(2)}(t)p^{(1)}(t+\tau_1)p^{(1)}(t+\tau_2)\}. \quad (7)$$

Hasselmann et al. (1963) examined third-order statistics of pressure records of swell in relatively shallow water, through the bottom-pressure bispectrum $B_b(f_1, f_2)$ defined as the Fourier transform of $R_b(\tau_1, \tau_2)$:

$$B_b(f_1, f_2) \equiv 2\int_{-\infty}^{\infty} d\tau_1 \int_{-\infty}^{\infty} d\tau_2 R_b(\tau_1, \tau_2) \times \exp[-2\pi i(f_1\tau_1 + f_2\tau_2)] = 2\frac{\mathrm{E}\{dP(f_1)dP(f_2)dP^*(f_1+f_2)\}}{df_1 df_2} \quad (8)$$

where $*$ denotes the complex conjugate and $dP(f)$ is the Fourier–Stieltjes transform of $p(t)$

$$p(t) = \int_{-\infty}^{\infty} dP(f) \exp(2\pi i f t). \quad (9)$$

Estimates of $B_b(f_1, f_2)$ are conveniently normalized by the bottom-pressure spectral density at frequencies f_1, f_2, and $f_1 + f_2$,

$$b(f_1, f_2) \equiv \frac{B_b(f_1, f_2)}{[E_b(f_1)E_b(f_2)E_b(f_1+f_2)]^{1/2}} \quad (10)$$

where [analogous to Eq. (8)]

$$E_b(f) \equiv 2\,\mathrm{E}\{dP(f)dP^*(f)\}/df.$$

When nondimensionalized by the frequency bandwidth, $|b(f_1, f_2)|$ is often called "bicoherence" in digital bispectral analysis (e.g., Kim and Powers 1979; Elgar and Guza 1985).

To fourth order in wave steepness, only triad interactions between all possible combinations of one secondary- and two primary-wave components with frequencies f_1, f_2 and $f_1 + f_2$ contribute to $B_b(f_1, f_2)$. In 13-m depth, the dominant contributions to $B_b(f_1, f_2)$ for $f_1 + f_2$ in approximately the range 0.35–0.60 Hz are triads consisting of two free waves with frequencies f_1 and f_2, and a forced wave with the sum frequency $f_1 + f_2$ [Eqs. (7) and (8); appendix B, Eqs. (B1) and (B2)]

$$B_b(f_1, f_2) \approx \int_0^{2\pi} d\theta_1 \int_0^{2\pi} d\theta_2 D(f_1, f_2, \Delta\theta) \times E_{b,\mathrm{free}}(f_1, \theta_1)E_{b,\mathrm{free}}(f_2, \theta_2) \quad (11)$$

and $E_b(f_1 + f_2)$ is approximately the secondary-wave spectrum (HG1),

$$E_b(f_1+f_2) \approx \int_0^{f_1+f_2} df \int_0^{2\pi} d\theta_1 \int_0^{2\pi} d\theta_2 D^2(f_1+f_2-f, f, \Delta\theta) \times E_{b,\mathrm{free}}(f_1+f_2-f, \theta_1)E_{b,\mathrm{free}}(f, \theta_2). \quad (12)$$

If $E_{b,\mathrm{free}}(f, \theta)$ is directionally narrow at frequencies f_1 and f_2 [i.e., if the interaction coefficient D is approximately constant for (θ_1, θ_2) free-wave pairs contributing to $E_b(f_1)E_b(f_2)$], then $|b(f_1, f_2)|$ can be interpreted as a relative measure of nonlinear coupling between forced waves with frequency $f_1 + f_2$ and free-wave pairs with frequencies f_1 and f_2. In general, however, wavenumber triads with different D contribute to $b(f_1, f_2)$, and directional spreading of wind waves will tend to reduce $|b(f_1, f_2)|$ [Eqs. (10), (11), and (12)]. In fact, since the interaction coefficient D can take both positive values (e.g., colinear free waves) and negative values (e.g., opposing free waves), depending on the water depth and the propagation directions of the interacting free waves (HG1), it is theoretically possible that contributions from different wavenumber triads (at the same f_1, f_2) cancel and $b(f_1, f_2)$ vanishes despite strong nonlinear coupling of the frequencies f_1, f_2 and $f_1 + f_2$. However, bispectral analysis is qualitatively useful in the sense that large negative or positive values of $b(f_1, f_2)$ estimates identify nonlinear interactions. The bispectra estimates presented in section 4 are used to supplement and independently confirm earlier conclusions based on second-order statistics, discussed in HG1 and section 2 of the present study.

Also of interest to the sum interactions of sea and swell is the integral of the bispectrum for constant sum frequency $b_i(f)$ [normalized by the second-order spectrum analogous to Eq. (10)], defined as

$$b_i(f) \equiv \frac{\int_0^f df' B_b(f-f', f')}{\left[\int_0^f df' E_b(f-f')E_b(f')E_b(f)\right]^{1/2}}. \quad (13)$$

At double sea frequencies ($f \approx 0.35$–0.60 Hz) where sea floor pressure is theoretically dominated by relatively weakly attenuated forced secondary waves, $b_i(f)$ is essentially a bulk measure of nonlinear coupling between forced waves with frequency f and all possible pairs of free waves with sum frequency f, and is approximately given by [Eqs. (11) and (12)]

$$b_i(f) \approx \frac{D_1(f)}{[D_0(f)D_2(f)]^{1/2}} \qquad (14)$$

with $D_n(f)$ the moments

$$D_n(f) \equiv \int_0^f df' \int_0^{2\pi} d\theta_1 \int_0^{2\pi} d\theta_2 D^n(f-f', f', \Delta\theta) \times E_{b,\text{free}}(f-f', \theta_1) E_{b,\text{free}}(f', \theta_2). \qquad (15)$$

From Eqs. (14) and (15) it follows that $-1 < b_i(f) < 1$. If all the energy at frequency f is forced and the interaction coefficient D is constant for all contributing wave triads, then $b_i^2(f) = 1$. Both variations in D and the presence of free-wave energy or other motions (e.g., turbulence) at frequency f will reduce $b_i^2(f)$ [as they would reduce $b^2(f-f', f')$, Eqs. (10)–(12)]. Thus, $b_i^2(f)$ can be interpreted as a lower bound on the fraction of energy at frequency f that is nonlinearly coupled to sea and swell.

In the present study, only univariate third-order statistics of the bottom-pressure time series are considered [i.e., the auto-bispectra, Eqs. (6) and (8)]. Analogous to cross-spectra, cross-bispectra can be defined as the Fourier transforms of the third-order cross-correlation functions of the time series of the array elements (e.g., Elgar and Guza 1985). Through multivariate analysis of third-order statistics, the coupling between free and forced waves may be examined in greater detail in the wavenumber–frequency domain. Such work is planned using data collected recently with a more extensive array of sea-floor pressure sensors.

4. Observed coupling between free and forced waves

The normalized bispectrum $b(f_1, f_2)$ [Eq. (10)] and the normalized integrated bispectrum $b_i(f)$ [Eq. (13)] were estimated from the sea-floor pressure data for each of the three data runs. First, the spectra $B_b(f_1, f_2)$ and $E_b(f)$ were estimated for every individual sensor in the bottom array (Fig. 4), based on the Fourier transforms of overlapping, detided and tapered, 34.1-minute data segments. Statistical stability of the spectral estimates was achieved by merging 25 neighboring frequency bands (i.e., 25^2 bands in $f_1 - f_2$ space) and averaging the ensembles. Finally, estimates of $b(f_1, f_2)$ and $b_i(f)$ were obtained by substituting the spatially averaged $B_b(f_1, f_2)$ and $E_b(f)$ (i.e., the ensemble average of the spectra computed for the individual instruments) in Eqs. (10) and (13). The results (Figs. 9, 10, and 11) correspond to the $E_b(f)$ and $E_{s,\text{free}}(f, \theta)$ estimates in Figs. 1, 2, and 3, respectively, and the $k_{\text{rms}}(f)$ and $\theta_{\text{mean}}(f)$ estimates in Figs. 5, 6, and 7, respectively. Theoretical predictions of $b(f_1, f_2)$ and $b_i(f)$ in the sum frequency range 0.3–0.5 Hz, based on Eqs. (10)–(12) and (14), respectively (i.e., assuming that all energy at the sum frequency is forced), are included in Figs. 9, 10, and 11.

On all three days, the imaginary parts in the observed $b(f_1, f_2)$ and $b_i(f)$ are very small (Figs. 9, 10, and 11) and are scattered more or less randomly about zero (Figs. 9b, 10b, and 11b), consistent with weakly nonlinear wave theory. Since the nonlinear interaction coefficient D is real for all possible free-wave pairs [ap-

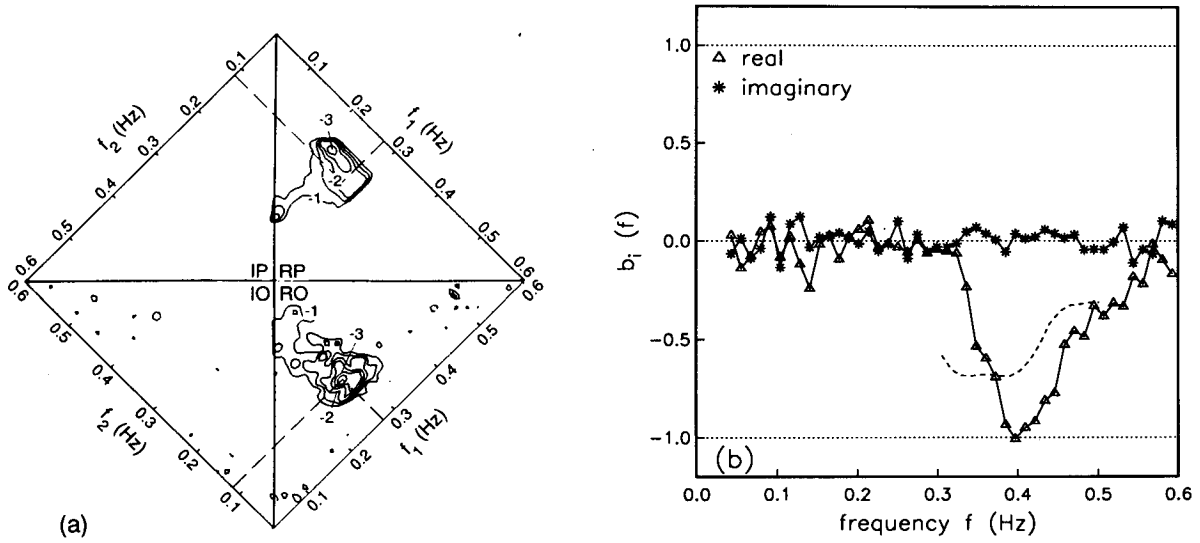

FIG. 9. Observed and predicted sea floor pressure bispectra on 11 October 1988. (a) Contours of the normalized bispectrum $b(f_1, f_2)$ [Eq. (10)] at levels ± 1, 1.5, 2, 2.5, 3, 3.5, 4, 4.5, and 5 $\text{Hz}^{-1/2}$. Solid and dashed contours correspond to negative and positive values of $b(f_1, f_2)$, respectively. Sectors marked RO and IO show the observed real and imaginary parts of $b(f_1, f_2)$, respectively, and sectors marked RP and IP the theoretically predicted [Eqs. (11) and (12)] real and imaginary parts, respectively. The dashed lines indicate the frequencies f_1 and f_2 where the observed $|b(f_1, f_2)|$ is maximum. (b) The solid curves are the observed real and imaginary parts of the normalized (dimensionless) integrated bispectrum $b_i(f)$ [Eq. (13)], and the dashed curve is a theoretical prediction of $b_i(f)$, assuming that all energy at frequency f is forced [Eq. (14), the imaginary part theoretically vanishes].

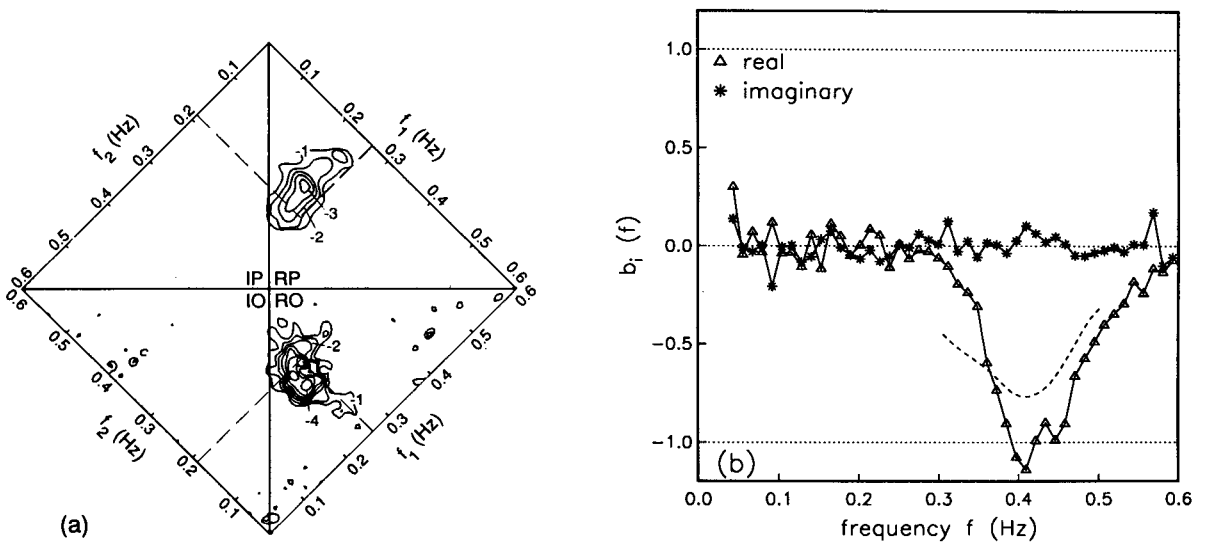

FIG. 10. As in Fig. 9 but on 12 October 1988.

pendix B, Eq. (B3)], the imaginary part of the bispectrum theoretically vanishes and the real part is nonzero [Eqs. (7) and (8); appendix B], which means that the bottom-pressure field is statistically skewed about a horizontal plane but symmetric about any vertical plane (i.e., wave crests are not pitched forward or backward). Wave-generation effects, not accounted for in weakly nonlinear wave theory, are a possible source for asymmetry of natural wind wave profiles (i.e., steep forward faces) causing negative imaginary parts of the bispectrum (e.g., Masuda and Kuo 1981a). The small imaginary parts of bispectra observed in the present study suggest that wind wave statistics at the sea floor (where high wavenumber components are attenuated) are not significantly affected by wave generation effects, in contrast to surface elevation measurements by Masuda and Kuo (1981b) in a laboratory experiment with similar (but directionally narrower) actively generated deep-water wind waves that show imaginary parts of bispectral estimates as large as 50% of the real parts.

In contrast to the small imaginary parts of the $b(f_1, f_2)$ and $b_i(f)$ estimates, the real parts show relatively large, consistently negative values at sum frequencies > 0.3 Hz. The observed negative sign of the bispectra

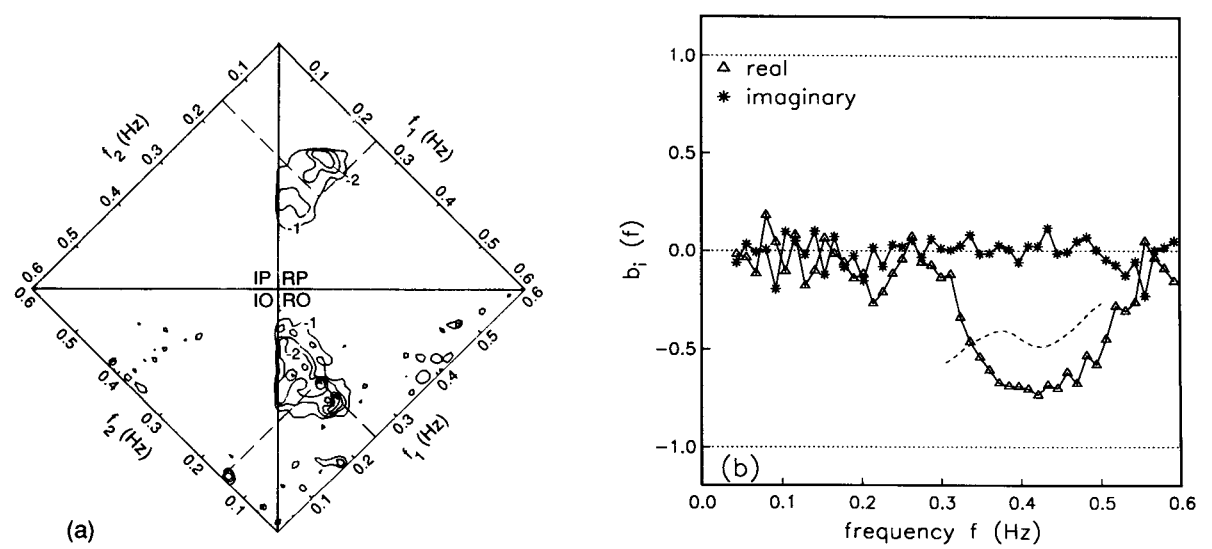

FIG. 11. As in Fig. 9 but on 13 October 1988.

is consistent with theory since the coefficient D is negative for relatively long wavelength forced waves excited by sum interactions of directionally opposing free waves (HG1). The opposing free-wave interactions observed in relatively deep water thus contribute a negative skewness to the sea-floor pressure field, as opposed to the positive skewness (i.e., positive D) observed by Hasselmann et al. (1963) for colinear free-wave interactions ("Stokes harmonics") in relatively shallow water.

On all three days the predicted and observed $b(f_1, f_2)$ are qualitatively similar with a broad negative (real) peak at about the same frequencies (Figs. 9a, 10a, and 11a), and the observed $b_i(f)$ are in good agreement with the predictions for $f > 0.35$ Hz where free-wave contributions to $E_b(f)$ are expected to be negligibly small (Figs. 9b, 10b, and 11b). The predicted $|b(f_1, f_2)|$ and $|b_i(f)|$ are consistently somewhat smaller than the observed values, possibly because the true directional spectrum of free waves is generally narrower than the estimate extracted from the middepth pressure array using a smoothness optimization technique (Herbers and Guza 1990; HG1). Hence, because of the larger variations of the coefficient D for a relatively broad estimate of $E_{b,\text{free}}(f, \theta)$, predictions of $|b(f_1, f_2)|$ and $|b_i(f)|$ will tend to be biased low [Eqs. (10)–(15)]. On all three days the predicted peak frequencies of $b(f_1, f_2)$ are somewhat lower than the observed peak frequencies, possibly because the (negative) bias in $|b(f_1, f_2)|$ predictions due to errors in $E_{b,\text{free}}(f, \theta)$ estimates are generally smaller at lower frequencies where D is less sensitive to $\Delta\theta$ (HG1). Additionally, for $f_1 + f_2 < 0.35$ Hz, predictions of $|b(f_1, f_2)|$ may be biased high because of neglected free-wave contributions to $E_b(f_1 + f_2)$ [Eqs. (10) and (12)].

The $b(f_1, f_2)$ observed on 11 October (Fig. 9a) shows a peak at frequencies $f_1 \approx 0.27$ Hz and $f_2 \approx 0.12$ Hz that corresponds to nearly directionally opposing sea and swell peaks in $E_{s,\text{free}}(f, \theta)$ (Fig. 1b). The corresponding $b_i(f)$ estimate reaches a minimum value of about -1 at the sum frequency (Fig. 9b), confirming that all the energy at $f \approx 0.4$ Hz is forced by nonlinear sea and swell interactions. Note that this maximum value of $|b_i(f)|$ is at a frequency ($\approx$0.4 Hz) well below the peak frequency of the forced-wave energy spectrum ($\approx$0.5 Hz, Fig. 1a). For sum frequencies close to the forced-wave spectral peak, the observed and predicted $|b(f_1, f_2)|$ levels are relatively low (Fig. 9a). The good agreement between the observed and predicted $b_i(f)$ (both are about -0.3 at $f = 0.5$ Hz, Fig. 9b) suggests that these low bispectral levels are not caused by the presence of high-frequency pressure fluctuations that are not coupled to sea and swell (for example, turbulence), but rather the result of appreciable variations of the coefficient D over the broad range of interacting wavenumber triads. The observed and predicted low bispectral levels in Fig. 9, at double sea sum frequencies dominated by forced waves, illustrate that nonlinear coupling of surface waves may not always be detectable in bispectra of broad directional seas.

On 12 October (Fig. 10a) the $b(f_1, f_2)$ estimate shows a similar broad peak at $f_1 \approx 0.26$ Hz and $f_2 \approx 0.19$ Hz, corresponding to directionally opposing seas in the $E_{s,\text{free}}(f, \theta)$ estimate (Fig. 2b). In this case, the sum frequency ($f \approx 0.45$ Hz), where $b_i(f)$ is again approximately equal to -1 (Fig. 10b), coincides with the peak of the forced-wave energy spectrum (Fig. 2a). Bispectral analysis thus shows strong phase coupling between this forced-wave peak and two relatively narrow [i.e., variations in D are small, Eqs. (10)–(15)] directionally opposing seas (Fig. 2b).

Finally, on 13 October (Fig. 11a) the shape of the bispectrum is somewhat more complicated. The observed $b(f_1, f_2)$ shows statistically significant real, negative values for a wide f_1, f_2 range with peak values at $f_1 \approx 0.24$ Hz, $f_2 \approx 0.11$ Hz (interactions between seas from the northwest and swell from the southeast, Fig. 3b) and $f_1 \approx 0.25$ Hz, $f_2 \approx 0.15$ Hz (interactions between seas from the northwest and northeast, Fig. 3b). A broad range of free-wave frequencies and directions (Fig. 3b) contribute to the 0.4-Hz forced-wave peak in $E_b(f)$, consistent with a $|b_i(f)|$ estimate and prediction smaller than 1 (Fig. 11b).

A bispectrum estimate obtained from surface elevation measurements on 12 October (not shown; data provided by A. T. Jessup, personal communication) did not indicate statistically significant nonlinear coupling between sea and swell waves, possibly because free waves dominate the surface elevation spectrum over a wide-frequency range.

In summary, the observed third-order statistics support the conclusions based on second-order (cross-) spectral analysis presented in HG1 and section 2 of this paper. Bispectral estimates (Figs. 9, 10, and 11) show that the observed double sea frequency sea-floor pressure fluctuations are nonlinearly coupled to nearly directionally opposing seas and swell, and the phase relationship between the interacting components is consistent with weakly nonlinear theory (Hasselmann 1962).

5. Summary and conclusions

This is Part 2 of a study of nonlinear effects on natural wind-generated surface gravity waves, using data from two arrays of pressure transducers (one at middepth and one on the sea floor) deployed in 13-m depth at the Chesapeake Light Tower, located 30 km offshore of Norfolk, Virginia, in fall 1988 as part of the SAXON Experiment. In Part 1 (Herbers and Guza 1991) it was shown that sea-floor pressure fluctuations observed at double wind-wave frequencies are forced secondary waves, excited by nonlinear interactions between nearly directionally opposing seas and swell (Figs. 1, 2, and 3). Observed forced-wave energy levels agree well with predictions, based on weakly nonlinear wave theory

(Hasselmann 1962) and estimates of the surface elevation frequency–directional spectrum $E_{s,\text{free}}(f, \theta)$ (obtained from the middepth array). In the present study (Part 2), the sea-floor pressure array data is used to examine the wavelengths and propagation directions of forced waves and the non-Gaussian statistics associated with the nonrandom phase relationship between free and forced waves.

Since forced waves do not obey a dispersion relation, their directional properties cannot be examined with conventional directional spectra estimation techniques. Although the six-element sea floor pressure array deployed during SAXON (Fig. 4) is not suitable for estimation of the full wavenumber–frequency spectrum, owing to its compact geometry, this array can provide approximately unbiased estimates of a root-mean-square wavenumber magnitude k_{rms} [Eq. (2)] and a vector-averaged mean wave propagation direction θ_{mean} [Eq. (3)], both functions of frequency. The method, based on an expansion for small sensor separations relative to the wavelength, can be used to verify the dispersion relation of free waves and examine the mean wavelengths and propagation directions of forced waves.

Estimates of k_{rms} and θ_{mean} were extracted from the bottom-pressure array data on 11, 12, and 13 October, when forced-wave energy levels were relatively high (Figs. 5, 6, and 7). In the frequency range 0.05–0.30 Hz, the k_{rms} estimates are within 10% of the linear dispersion relation (Fig. 8), demonstrating that this frequency range is dominated by free sea and swell waves. The θ_{mean} estimates in the free-wave range 0.05–0.30 Hz agree very well with independent estimates obtained from the middepth array data through integration of $E_{s,\text{free}}(f, \theta)$ (calculated assuming linear theory). At frequencies higher than about 0.35 Hz, free surface gravity waves are very strongly attenuated at the sea floor, and forced waves are theoretically expected to dominate the pressure observations. The k_{rms} estimates show a clear transition between a free-wave regime ($f < 0.30$ Hz), where sea-floor pressure fluctuations obey the dispersion relation, and a forced-wave regime ($f > 0.35$ Hz), where the observed wavelengths are much longer than predicted from the dispersion relation. Good agreement between the observed k_{rms} and θ_{mean} at double sea frequencies (0.35–0.50 Hz), and predictions based on weakly nonlinear theory and $E_{s,\text{free}}(f, \theta)$ estimates, confirms that the observed forced pressure fluctuations have the theoretically expected sum vector wavenumber of the interacting wind waves.

Statistics of weakly nonlinear surface gravity waves are theoretically non-Gaussian because of a consistent phase relationship between interacting primary and secondary wave components. Following Hasselmann et al. (1963), bottom-pressure bispectra are used to examine phase coupling between (primary) sea and swell waves and the associated sum frequency secondary waves. The magnitude of the normalized bispectrum $b(f_1, f_2)$ [Eq. (10)] can be interpreted as a relative measure of phase coupling between waves at frequencies f_1, f_2 and $f_1 + f_2$. However, for directionally broad wind-driven seas normalized bispectral levels may be greatly reduced by variations of the nonlinear interaction coefficient over wavenumber triads contributing to $b(f_1, f_2)$. Thus, low bispectral levels do not necessarily imply the dominance of statistically independent free waves. Nonetheless, the analysis is useful because the bispectrum vanishes for a Gaussian process. Statistically significant deviations of $b(f_1, f_2)$ from zero are due to wave nonlinearity and yield qualitative insight into the free-wave components involved in forced-wave generation. Additionally, a normalized integral of the bispectrum for constant sum frequency, $b_i(f)$ [Eq. (13)], is shown to be a lower bound on the fraction of the energy at frequency f that is phase coupled to all possible free-wave pairs.

The observed bispectra (Figs. 9, 10, and 11) all have small imaginary parts scattered about the theoretical value zero and relatively large negative real parts that are qualitatively consistent with predictions based on weakly nonlinear theory and the $E_{s,\text{free}}(f, \theta)$ estimates. On all three occasions the peak of the $b(f_1, f_2)$ estimate is at frequencies corresponding to nearly directionally opposing sea and swell peaks in the $E_{s,\text{free}}(f, \theta)$ estimate. Peak values of $b_i(f)$ estimates close to -1 confirm the strong phase coupling between free and forced waves. On one occasion, however, nonlinear coupling between directionally broad seas and sum frequency forced waves is barely detectable in the bispectrum, consistent with the theoretical prediction ($f = 0.5$ Hz in Fig. 9b). The observed third-order statistics $b(f_1, f_2)$ and $b_i(f)$ strongly support earlier conclusions of this study based on second-order statistics.

Acknowledgments. This research was sponsored by the Remote Sensing Program (Grants N00014-87-C-0127 and N00014-89-J-3097) of the Office of Naval Research (Ocean Engineering Division). The patience and confidence of ONR Science Officers H. Dolezalek and Dr. F. Herr is gratefully acknowledged. THCH received additional support from the Office of Naval Research Geology and Geophysics Program and under Grant N00014-86-K-0789. The staff of the Center for Coastal Studies (Scripps Institution of Oceanography), led by R. L. Lowe, W. A. Boyd, and M. C. Clifton, installed and maintained the arrays. We thank the anonymous reviewers for useful suggestions and Dr. S. Elgar for helpful discussions on bispectra and for generously sharing his code with us.

APPENDIX A

Estimation of Average Wavenumbers

The technique developed here for estimating k_{rms} and θ_{mean} is an extension of a method for estimating wave radiation stresses and energy fluxes from a square four-element array (Herbers and Guza 1989). The

cross-spectrum $H_{pq}(f)$ of a pair of array components with indices p and q is related to $E_b(f, k, \theta)$ by

$$H_{pq}(f) = \int_0^\infty dk \int_0^{2\pi} kd\theta \exp[ik(\cos(\theta)x_{pq} + \sin(\theta)y_{pq})]E_b(f, k, \theta) \quad \text{(A1)}$$

where x_{pq} ($=x_p - x_q$) and y_{pq} ($=y_p - y_q$) are the x and y lags, respectively, between instruments p (at $\mathbf{x}_p = [x_p, y_p]$) and q (at $\mathbf{x}_q = [x_q, y_q]$) (Fig. 4). According to theory, free- and forced-wave components with wavelengths comparable to the water depth (13 m) are attenuated by about 10^5 in energy at the sea floor (e.g., Hasselmann et al. 1963). Thus, the sea-floor pressure observations are generally expected to be dominated by waves with wavelengths that are long compared to both water depth and sensor separations, and Eq. (A1) can be expanded for small kx_{pq}, ky_{pq}

$$H_{pq}(f) = \sum_{n=0}^{\infty} \frac{1}{n!} \int_0^\infty dk \int_0^{2\pi} kd\theta[ik(\cos(\theta)x_{pq} + \sin(\theta)y_{pq})]^n E_b(f, k, \theta). \quad \text{(A2)}$$

The following linear combinations of normalized co-spectra C_{pq} and quadrature-spectra Q_{pq}

$$C_{pq}(f) - iQ_{pq}(f) \equiv \frac{H_{pq}(f)}{[H_{pp}(f)H_{qq}(f)]^{1/2}} \quad \text{(A3)}$$

are formed using Eq. (A2), in order to obtain approximately unbiased estimators for $k_{\text{rms}}(f)$ [Eq. (2)] and $\theta_{\text{mean}}(f)$ [Eq. (3)]:

$$\sum_{p,q} a_{pq}C_{pq}(f) \int_0^\infty dk \int_0^{2\pi} kd\theta[(kL)^2 - \tfrac{1}{90}(kL)^6 + \mathrm{O}(kL)^8]E_b(f, k, \theta) = \frac{}{\int_0^\infty dk \int_0^{2\pi} kd\theta E_b(f, k, \theta)} \quad \text{(A4a)}$$

$$\sum_{p,q} b_{pq}C_{pq}(f) \int_0^\infty dk \int_0^{2\pi} kd\theta[(kL)^4 - \tfrac{1}{6}(kL)^6 + \mathrm{O}(kL)^8]E_b(f, k, \theta) = \frac{}{\int_0^\infty dk \int_0^{2\pi} kd\theta E_b(f, k, \theta)} \quad \text{(A4b)}$$

$$\sum_{p,q} c_{pq}Q_{pq}(f) \int_0^\infty dk \int_0^{2\pi} kd\theta[kL\cos(\theta) - \tfrac{1}{30}(kL)^5 \times \cos(\theta) + \mathrm{O}(kL)^7]E_b(f, k, \theta) = \frac{}{\int_0^\infty dk \int_0^{2\pi} kd\theta E_b(f, k, \theta)} \quad \text{(A4c)}$$

$$\sum_{p,q} d_{pq}Q_{pq}(f) \int_0^\infty dk \int_0^{2\pi} kd\theta[kL\sin(\theta) - \tfrac{1}{30}(kL)^5 \times \sin(\theta) + \mathrm{O}(kL)^7]E_b(f, k, \theta) = \frac{}{\int_0^\infty dk \int_0^{2\pi} kd\theta E_b(f, k, \theta)} \quad \text{(A4d)}$$

where L is the smallest sensor separation in the array (6 m) and the coefficients a_{pq}, b_{pq}, c_{pq}, and d_{pq} are listed in Table A1. Equations (A4a)–(A4d) can be combined to yield accurate expressions for k_{rms} and θ_{mean}

$$k_{\text{rms}}(f) \approx \frac{1}{L}\left[\sum_{p,q} a_{pq}C_{pq}(f)\left(1 + \frac{1}{90}\sum_{p,q} b_{pq}C_{pq}(f)\right)\right]^{1/2} \quad \text{(A5a)}$$

$$\tan[\theta_{\text{mean}}(f)] \approx \frac{\sum_{p,q} d_{pq}Q_{pq}(f)}{\sum_{p,q} c_{pq}Q_{pq}(f)}. \quad \text{(A5b)}$$

The leading bias terms in Eq. (A5) are $\mathrm{O}(kL)^4$ [Eq. (A4)]. These errors are extremely small for $kL < 1$ but increase rapidly for $kL > 1.5$.

The range of wavelengths expected at the sea floor in 13-m depth is large. Free sea and swell waves obeying the dispersion relation [Eq. (1)] have wavelengths ranging from about 15 m for the highest frequency (0.32 Hz) seas that reach the sea floor to 220 m for extremely low-frequency (0.05 Hz) swell. For the frequency range 0.08–0.25 Hz, the minimum sensor separation L = 6 m of the present array (Fig. 4) is small

TABLE A1. Coefficients of wavenumber estimators [Eq. (A5)].

Sensor pair	Coefficients			
	a	*b*	*c*	*d*
P_8, P_8	95/132	145/66	0	0
P_8, P_{10}	−2/11	2/11	−1/15	−1/15
P_8, P_{11}	−2/11	2/11	1/15	−1/15
P_8, P_{12}	−2/11	2/11	1/15	1/15
P_8, P_{13}	−2/11	2/11	−1/15	1/15
P_8, P_{14}	−64/33	−96/11	−16/15	0
P_{10}, P_{10}	95/132	145/66	0	0
P_{10}, P_{11}	2/33	17/22	−1/15	0
P_{10}, P_{12}	1/44	5/22	−1/60	−1/60
P_{10}, P_{13}	2/33	17/22	0	−1/15
P_{10}, P_{14}	−32/33	−48/11	0	8/15
P_{11}, P_{11}	95/132	145/66	0	0
P_{11}, P_{12}	2/33	17/22	0	−1/15
P_{11}, P_{13}	1/44	5/22	1/60	−1/60
P_{11}, P_{14}	0	0	0	0
P_{12}, P_{12}	95/132	145/66	0	0
P_{12}, P_{13}	2/33	17/22	1/15	0
P_{12}, P_{14}	0	0	0	0
P_{13}, P_{13}	95/132	145/66	0	0
P_{13}, P_{14}	−32/33	−48/11	0	−8/15
P_{14}, P_{14}	95/132	145/66	0	0

enough compared to free wavelengths ($kL < 1.5$) that estimates of k_{rms} and θ_{mean} are expected to be approximately unbiased and large enough ($kL > 0.3$) that these estimates are relatively insensitive to measurement errors. For higher-frequency seas, the sensor separations are somewhat large; the $O(kL)^4$ bias terms in Eq. (A5) are O(1) for 0.32-Hz free waves ($kL = 2.5$). However, through the particular choice of the coefficients a_{pq} and b_{pq} for k_{rms} (c_{pq} and d_{pq} for θ_{mean}), the (lowest order) $O(kL)^4$ bias errors contributed by Eqs. (A4a) and (A4b) [Eqs. (A4c) and (A4d)] are independent of θ and tend to cancel if the (nondirectional) $f - k$ spectrum

$$E_b(f, k) \equiv \int_0^{2\pi} k d\theta E_b(f, k, \theta)$$

is narrow. Hence, bias errors in Eq. (A5) are $O(kL)^6$ at frequencies dominated by free waves obeying the linear dispersion relation [Eq. (1)], and simulations for realistic directional spectra of wind waves suggest that the $O(kL)^6$ bias is not unacceptably large for the shortest-wavelength free waves ($\approx$0.32 Hz) that reach the sea floor. In the frequency range 0.05–0.08 Hz, the wavelengths of free swell are long compared to the sensor spacings ($kL = 0.17$–0.28), and estimates of k_{rms} and θ_{mean} are possibly somewhat degraded by measurement errors.

Forced waves generated by sum interactions of sea and swell theoretically can have any wavelength longer than a free wave of the same frequency. However, for the typically broad $E_{s,free}(f, \theta)$ expected for natural wind-driven seas (0.1–0.35 Hz), the dominant sum frequency (0.2–0.7 Hz) forced secondary waves at the sea floor in 13-m depth have wavelengths ranging roughly from about 25 to 150 m. Contributions of shorter forced waves (wavelengths < 25 m, i.e., comparable to or smaller than the water depth) are small at the sea floor because of their strong vertical decay, whereas longer double sea–frequency forced waves (wavelengths > 150 m, i.e., much longer than the interacting free waves) are also generally small because they are generated only by pairs of approximately directionally opposing free waves of equal frequency ($f_1 \approx f_2$; $|\theta_1 - \theta_2| \approx 180°$) and there is typically little such opposing energy. At double swell frequencies (0.1–0.2 Hz), colinear free-wave interactions ($\theta_1 \approx \theta_2$) are theoretically expected to dominate the forced-wave field because 0.05–0.1-Hz remotely generated swell is generally directionally narrow, and the associated Stokes harmonics with wavelengths ranging from about 50 m to 110 m are both amplified by near-resonance and only weakly attenuated at the sea floor in 13-m depth (HG1). Thus, the range of wavenumbers of the dominant forced waves at double sea and swell frequencies is generally limited to about $0.25 < kL < 1.5$, and errors in k_{rms} and θ_{mean} estimates due to both measurement inaccuracies and a finite kL bias are expected to be relatively small.

APPENDIX B

Cross-Spectra of Weakly Nonlinear Sea Floor Pressure

The primary bottom-pressure field $p^{(1)}(\mathbf{x}, t)$ can be expressed in terms of the Fourier-Stieltjes transform $dP(\mathbf{k})$ as (e.g., Hasselmann 1962)

$$p^{(1)}(\mathbf{x}, t) = \int_{\mathbf{k}} \exp[i\mathbf{k}\cdot\mathbf{x}][dP_-^{(1)}(\mathbf{k}) \exp[i2\pi ft] + dP_+^{(1)}(\mathbf{k}) \exp[-i2\pi ft]] \quad \text{(B1)}$$

where $dP_-^{(1)}(\mathbf{k})$ is the complex conjugate of $dP_+^{(1)}(-\mathbf{k})$ and f is given by the dispersion relation [Eq. (1)]. The secondary bottom-pressure field $p^{(2)}(\mathbf{x}, t)$ is given by

$$p^{(2)}(\mathbf{x}, t) = \int_{\mathbf{k}_1}\int_{\mathbf{k}_2} \exp[i(\mathbf{k}_1 + \mathbf{k}_2)\cdot\mathbf{x}] \times \sum_{s_1,s_2=\pm 1} D(s_1f_1, s_2f_2, \Delta\theta) dP_{s_1}^{(1)}(\mathbf{k}_1) dP_{s_2}^{(1)}(\mathbf{k}_2) \times \exp[-i2\pi(s_1f_1 + s_2f_2)t] \quad \text{(B2)}$$

where $\Delta\theta = |\theta_1 - \theta_2|$ is the difference in propagation direction of the interacting pair of primary wave components $(s_1f_1, \mathbf{k}_1)$ and $(s_2f_2, \mathbf{k}_2)$ [with $\mathbf{k}_i = (k_i \cos\theta_i, k_i \sin\theta_i)$ and k_i given by the dispersion relation, Eq. (1)] and D is the interaction coefficient,

$$D(s_1f_1, s_2f_2, \Delta\theta) \equiv -\frac{gk_1k_2\cos(\Delta\theta)}{2\sigma_1\sigma_2} + \frac{g(\sigma_1+\sigma_2)\cosh(k_1h)\cosh(k_2h)}{[gk_3\tanh(k_3h) - (\sigma_1+\sigma_2)^2]\sigma_1\sigma_2\cosh(k_3h)} \times \left\{(\sigma_1+\sigma_2)\left[\frac{(\sigma_1\sigma_2)^2}{g^2} - k_1k_2\cos(\Delta\theta)\right] - \frac{1}{2}\left[\frac{\sigma_1k_2^2}{\cosh^2(k_2h)} + \frac{\sigma_2k_1^2}{\cosh^2(k_1h)}\right]\right\}, \quad \text{(B3)}$$

with $\sigma_i \equiv 2\pi s_i f_i$ and $k_3 = |\mathbf{k}_1 + \mathbf{k}_2|$. The dependence of the interaction coefficient C between secondary sea floor pressure and primary sea surface elevation [$C = (\cosh[k_1h]\cosh[k_2h])^{-1}D$] on the water depth and free-wave frequencies and propagation directions is discussed in HG1.

The cross-spectrum $H_{pq}(f)$ of sensors p and q[at $\mathbf{x}_p = (x_p, y_p)$ and $\mathbf{x}_q = (x_q, y_q)$, respectively, Fig. 4] can be expressed in terms of the frequency-directional spectrum of primary waves $E_{b,free}(f, \theta)$ [$\equiv 2\pi E\{dP_+^{(1)}(\mathbf{k})dP_-^{(1)}(-\mathbf{k})\}/(df d\theta)$] and the interaction coefficient D. To fourth order in wave steepness, $H_{pq}(f)$ is given by

$$H_{pq}(f) = 2\int_{-\infty}^{\infty} d\tau[\mathrm{E}\{p^{(1)}(\mathbf{x}_p, t)p^{(1)}(\mathbf{x}_q, t+\tau)\} + \mathrm{E}\{p^{(2)}(\mathbf{x}_p, t)p^{(2)}(\mathbf{x}_q, t+\tau)\} + \mathrm{E}\{p^{(1)}(\mathbf{x}_p, t)p^{(3)}(\mathbf{x}_q, t+\tau)\} + \mathrm{E}\{p^{(3)}(\mathbf{x}_p, t)p^{(1)}(\mathbf{x}_q, t+\tau)\}] \times \exp[-i2\pi f\tau] \quad \text{(B4)}$$

where $\mathrm{E}\{\ \}$ denotes the expected value and $p^{(3)}$ is the tertiary bottom-pressure field. For $f > 0.35$ Hz, the first, third, and fourth terms on the right-hand side of Eq. (B4) are negligibly small, owing to the strong attenuation at the sea floor of relatively short wavelength primary waves, and $H_{pq}(f)$ is theoretically dominated by relatively long wavelength secondary waves ($p^{(2)}$) excited by sum frequency interactions [$s_1 = s_2$ in Eqs. (B2) and (B3); see also HG1]. Substitution of $p^{(2)}$ [Eq. (B2)] in Eq. (B4), yields an expression for $H_{pq}(f)$ valid at high frequencies:

$$H_{pq,\,\mathrm{forced}}(f) \approx \int_0^f df' \int_0^{2\pi} d\theta_1 \int_0^{2\pi} d\theta_2 \times \exp\{i[(k_{f'}\cos(\theta_1) + k_{f-f'}\cos(\theta_2)]x_{pq} + [k_{f'}\sin(\theta_1) + k_{f-f'}\sin(\theta_2))y_{pq}]\} \times D^2(f', f-f', \Delta\theta)E_{b,\,\mathrm{free}}(f', \theta_1) \times E_{b,\,\mathrm{free}}(f-f', \theta_2), \quad \text{(B5)}$$

where $k_{f'}$ and $k_{f-f'}$ are the linear wavenumbers [Eq. (1)] at frequencies f' and $f-f'$, respectively, and x_{pq} ($=x_p - x_q$) and y_{pq} ($=y_p - y_q$) are the x and y lags, respectively, between instruments p and q.

REFERENCES

Cox, C. S., and D. C. Jacobs, 1989: Cartesian diver observations of double frequency pressure fluctuations in the upper levels of the ocean. *Geophys. Res. Lett.*, **16**(8), 807–810.

Donelan, M. A., J. Hamilton, and W. H. Hui, 1985: Directional spectra of wind-generated waves. *Phil. Trans. R. Soc. London*, **A315**, 509–562.

Elgar, S., and R. T. Guza, 1985: Observations of bispectra of shoaling surface gravity waves. *J. Fluid Mech.*, **161**, 425–448.

Goodman, D., T. Yamamoto, M. Trevorrow, C. Abbot, A. Turgut, M. Badiey, and K. Ando, 1989: Directional spectra observations of sea floor microseisms from an ocean-bottom seismometer array. *J. Acoust. Soc. Am.*, **86**, 2309–2317.

Hasselmann, K., 1962: On the non-linear energy transfer in a gravity-wave spectrum, Part 1. General theory. *J. Fluid Mech.*, **12**, 481–500.

——, 1963: A statistical analysis of the generation of microseisms. *Rev. Geophys.*, **1**(2), 177–210.

——, W. Munk, and G. MacDonald, 1963: Bispectra of ocean waves. *Times Series Analysis*, M. Rosenblatt, Ed., John Wiley, 125–139.

——, T. P. Barnett, E. Bouws, H. Carlsson, D. E. Cartwright, K. Enke, J. A. Ewing, H. Gienapp, D. E. Hasselmann, P. Kruseman, A. Meerburg, P. Müller, D. J. Olbers, K. Richter, W. Sell, and H. Walden, 1973: Measurements of wind wave growth and swell decay during the Joint North Sea Wave Project (JONSWAP). *Dtsch. Hydrogr. Z.* (Suppl.), **A8**(12), 1–95.

Herbers, T. H. C., and R. T. Guza, 1989: Estimation of wave radiation stresses from slope array data. *J. Geophys. Res.*, **94**(C2), 2099–2104.

——, and ——, 1990: Estimation of directional wave spectra from multicomponent observations. *J. Phys. Oceanogr.*, **20**, 1703–1724.

——, and ——, 1991: Wind–wave nonlinearity observed at the sea floor. Part I: Forced wave energy. *J. Phys. Oceanogr.*, **21**, 1740–1761.

Kim, Y. C., and E. J. Powers, 1979: Digital bispectral analysis and its application to nonlinear wave interactions. *IEEE Trans. Plasma Sci.*, **1**, 120–131.

Kinsman, B., 1965: *Wind Waves: Their Generation and Propagation on the Ocean Surface.* Prentice-Hall, 676 pp.

Komen, G. J., 1980: Nonlinear contributions to the frequency spectrum of wind-generated water waves. *J. Phys. Oceanogr.*, **10**, 779–790.

Laing, A. K., 1986: Nonlinear properties of random gravity waves in water of finite depth. *J. Phys. Oceanogr.*, **16**, 2013–2030.

Longuet-Higgins, M. S., 1950: A theory of the origin of microseisms. *Phil. Trans. R. Soc. London*, **A243**, 1–35.

——, 1963: The effect of non-linearities on statistical distributions in the theory of sea waves. *J. Fluid Mech.*, **17**(3), 459–480.

——, and R. W. Stewart, 1962: Radiation stress and mass transport in surface gravity waves with application to "surf beats." *J. Fluid Mech.*, **13**, 481–504.

Masuda, A., and Y-Y Kuo, 1981a: A note on the imaginary part of bispectra. *Deep-Sea Res.*, **28A**(3), 213–222.

——, and ——, 1981b: Bispectra for the surface displacement of random gravity waves in deep water. *Deep-Sea Res.*, **28A**(3), 223–237.

Miche, M., 1944: Movements ondulatoires de la mer en profondeur constante ou decroissante. *Ann. Ponts Chaussees*, **114**, 25–406.

Mitsuyasu, H., Y-Y Kuo, and A. Masuda, 1979: On the dispersion relation of random gravity waves. Part 2. An experiment. *J. Fluid Mech.*, **92**, 731–749.

Munk, W., F. Snodgrass, and F. Gilbert, 1964: Long waves on the continental shelf: An experiment to separate trapped and leaky modes. *J. Fluid Mech.*, **20**, 529–554.

Phillips, O. M., 1960: On the dynamics of unsteady gravity waves of finite amplitude. Part 1. The elementary interactions. *J. Fluid Mech.*, **9**, 193–217.

Webb, S. C., and C. S. Cox, 1986: Observations and modeling of seafloor microseisms. *J. Geophys. Res.*, **91**(B7), 7343–7358.